Energy stable and linearly well-balanced numerical schemes for the non-linear Shallow Water equations with Coriolis force

Emmanuel Audusse, Virgile Dubos, Noémie Gaveau, Yohan Penel

Energy stable and linearly well-balanced numerical schemes for the nonlinear Shallow Water equations with Coriolis force

Emmanuel Audusse * Virgile Dubos † Noémie Gaveau ‡ Yohan Penel §

June 28, 2023

Abstract

We analyse a class of energy-stable and linearly well-balanced numerical schemes dedicated to the nonlinear Shallow Water equations with Coriolis force. The proposed algorithms rely on colocated finite-volume approximations formulated on cartesian geometries. They involve appropriate diffusion terms in the numerical fluxes, expressed as discrete versions of the linear geostrophic equilibrium. We show that the resulting methods ensure semi-discrete energy estimates and numerical results show a very clear improvement around the nonlinear geostrophic equilibrium when compared to those of classic Godunov-type schemes.

1 Introduction

The question of the accuracy of numerical schemes for hyperbolic systems with source terms around stationary solutions and/or in asymptotic regimes has been a subject of great interest over the last two decades, see the seminal works [4,14,15] in late nineties and the reference books [6,13] ten years later. In the context of geophysical flows and for colocated finite-volume methods applied to shallow water equations, a lot of works have been devoted to the accuracy around the so-called lake-at-rest equilibrium and more recently extended to nonzero velocity one dimensional stationary states, see [5] and references therein. But for large scale atmospheric or oceanographic flows, the relevant stationary state is the geostrophic equilibrium, see [28] for a general introduction to geophysical rotating fluid dynamics. The accuracy of colocated finite-volume numerical schemes around such an equilibrium was less investigated. To our knowledge, the first work in this field is due to Bouchut, Le Sommer and Zeitlin [7], see also [8,9], but was fully accurate only for one-dimensional flows, as exhibited in [1]. Recently two independent works [19,27] proposed IMplicit-EXplicit type schemes for fully nonlinear equations which are proven to be accurate near the geostrophic equilibrium but, due to their implicit part, need to solve a global Laplace equation at each time step. Note that there exists also a lot of works devoted to the approximation of the Coriolis term in staggered finite-difference schemes, see for example [23] for a linear analysis and [22] for the fully nonlinear case and in the finite-element framework [20].

In this work, we aim at designing a explicit colocated finite-volume scheme that is proven to be accurate around the geostrophic equilibrium and stable in the nonlinear framework. Our work is based on the ideas developed in [1] where accurate and stable Godunov-type schemes were designed for the linear two-dimensional rotating wave equation but we will see in this paper that further developments are needed to handle the nonlinear case in a conservative way. All the numerical schemes we consider in this paper belong to the AUSM family where the flux is divided in an advective part and a pressure part, see the seminal works [17,18] and the recent review [11]. The first two ones involve a non conservative discretization of the pressure term but the last one is fully conservative.

The outline of the paper is as follows : in Section 2, we first introduce the system of equations under study and we characterise the geostrophic equilibrium. In Section 3, we define some discrete operators and we prove some of their properties. Equipped with these definitions, in Section 4, we can define our numerical schemes and study the two properties we are interested in: the decrease of the semi-discrete energy and the preservation of the geostrophic equilibrium in the linearised version. Note that all along the paper the term semi-discrete will refer to quantities

*LAGA, Institut Galilée, Université Sorbonne Paris Nord – 99 avenue Jean-Baptiste Clément, 93430 Villetaneuse.

†Laboratoire d'hydraulique Saint-Venant, EDF'lab Chatou – 6 quai Wattier, 78401 Chatou.

‡Institut Denis Poisson, Université d'Orléans, Université de Tours, CNRS UMR 7013, Route de Chartres, BP 6759, 45067 Orléans CEDEX 2.

§INRIA Paris – Sorbonne Université – CNRS (LJLL), team ANGE, 2 rue Simone Iff, CS 42112, 75589 Paris cedex 12.

that are discrete in space but continuous in time. Finally, in Section 5, we illustrate the behaviour of the schemes for some standard test cases and we exhibit a great improvement when compared to a classic finite-volume scheme.

2 Shallow water equations and geostrophic equilibrium

Let Ω be an open bounded domain of $\mathbb{R}^2$ and let $T > 0$. The nonlinear Shallow Water equations with Coriolis force formulated on $\Omega \times (0, T)$ read:

$$\begin{cases} \partial_t h + \operatorname{div}(h\boldsymbol{u}) = 0\,, \\ \partial_t (h\boldsymbol{u}) + \operatorname{div}(\boldsymbol{u} \otimes h\boldsymbol{u}) + h\nabla\phi = -\omega h \boldsymbol{u}^\perp\,, \end{cases} \tag{1}$$

where h is the water height and $\boldsymbol{u} = (u_x, u_y)$ the horizontal velocity, $\boldsymbol{u}^\perp = (-u_y, u_x)$ denoting its orthogonal vector in the (x, y) plane. The Coriolis force is accounted for in the momentum equations through the angular speed ω. Following [10, 21], the pressure forces appear under a non conservative form through the scalar potential $\phi = gh$, where g is the standard gravity constant. For the sake of simplicity, a flat topography is considered in the present work[1].
It is well-known that the total energy associated to System (1) decomposes as $E = E^p + E^k$ where

$$E^p = \frac{1}{2} g h^2 \quad \text{and} \quad E^k = \frac{1}{2} h \|\boldsymbol{u}\|^2$$

stand respectively for potential and kinetic energies. We recall that the energy E plays the role of a mathematical entropy associated to the hyperbolic system (1) and regular solutions satisfy the following conservation law

$$\partial_t E + \operatorname{div}\left[\left(\phi + \frac{1}{2}\|\boldsymbol{u}\|^2\right) h\boldsymbol{u}\right] = 0\,, \tag{2}$$

whereas for discontinuous solutions, the total energy is only non-increasing in time.
When developing numerical methods, main objectives are accuracy and stability. To get stability, a crucial objective is to build numerical approximations satisfying a discrete counterpart of (2) that ensures that the discrete energy is non-increasing. To achieve this, a general strategy is to consider a sufficient amount of numerical diffusion in the scheme. But in some physical contexts such as low Froude number regimes or near specific stationary states, these diffusive terms may considerably degrade the accuracy of the approximations and specific schemes are needed.
Here we are interested in flows around the geostrophic balance:

$$\nabla\phi + \omega \boldsymbol{u}^\perp = 0\,, \quad \operatorname{div} \boldsymbol{u} = 0\,. \tag{3}$$

To address such an issue, based on the study for the linear case [1], we propose a numerical approach involving discrete versions of these equilibria in the numerical fluxes. As a preliminary step, the strategy can be understood at the continuous level by investigating how Model (1) behaves with respect to some generic perturbations $(\boldsymbol{q}, \pi)$:

$$\begin{cases} \partial_t h + \operatorname{div}(h\boldsymbol{u} - \boldsymbol{q}) = 0\,, \\ \partial_t (h\boldsymbol{u}) + \operatorname{div}\left(\boldsymbol{u} \otimes (h\boldsymbol{u} - \boldsymbol{q})\right) + (h\nabla\phi - \nabla\pi) = -\omega\,(h\boldsymbol{u} - \boldsymbol{q})^\perp\,, \end{cases} \tag{4}$$

where $\boldsymbol{q}$ and π can be respectively seen as (small) perturbations with respect to the flow rate and to the hydrostatic pressure. Smooth solutions to the modified equations (4) satisfy the following energy balance:

$$\partial_t E + \operatorname{div}\left[\left(\phi + \frac{1}{2}\|\boldsymbol{u}\|^2\right)\ (h\boldsymbol{u} - \boldsymbol{q}) - \pi\boldsymbol{u}\right] = -\boldsymbol{q} \cdot \left(\nabla\phi + \omega\boldsymbol{u}^\perp\right) - \pi\ \operatorname{div}\boldsymbol{u}\,, \tag{5}$$

which motivates a choice for $\boldsymbol{q}$ and π involving respectively the quantities $\nabla\phi + \omega\,\boldsymbol{u}^\perp$ and $\operatorname{div}\boldsymbol{u}$. Let us remark that these quantities govern the geostrophic equilibrium (3) associated to System (1) linearised around the steady state $(\tilde{h}, \tilde{\boldsymbol{u}}) = (h_0, 0)$ for a constant h_0:

$$\begin{cases} \partial_t h = -h_0\ \operatorname{div}\boldsymbol{u}\,, \\ \partial_t \boldsymbol{u} = -(\nabla\phi + \omega\,\boldsymbol{u}^\perp)\,. \end{cases}$$

[1] In the case of a non-flat topography b, the present approach naturally extends by taking $\phi = g(h + b)$ and $E^p = \frac{1}{2} g h^2 + ghb$.

From a numerical point of view, diffusion terms are thus expected to have regularising effects in the sense that they allow to recover a discrete counterpart of (5). Moreover, such terms are intended to vanish close to the geostrophic equilibrium, which must improve the quality of the approximations in this regime. We implement this idea in a discrete setting in Section 4.3 and obtain a non-conservative scheme and a conservative one.

3 Discrete operators

3.1 Definition of the mesh

Let us first introduce some generic notations related to the discretisation of the equations. We consider a Cartesian tessellation $\mathcal{K}$ of the computational domain $\Omega \subset \mathbb{R}^2$ made of non-overlapping rectangular cells of sises $\Delta x \times \Delta y$. The set of all edges of the mesh is denoted by $\mathcal{E}$ and the set of vertices by $\mathcal{V}$.

- A generic cell of $\mathcal{K}$ is denoted by K and its boundary by ∂K. A given quantity Φ located on K is denoted by $\Phi_{i,j}$.
- A generic edge of $\mathcal{E}$ is denoted by e, its boundary by ∂e, its length by m_e and an arbitrary unit normal vector by $\boldsymbol{n}_e$. A given quantity Φ located on e is denoted by $\Phi_{i+1/2,j}$ (respectively $\Phi_{i,j+1/2}$) for y-axis (respectively x-axis) edge.
- Given a cell K and an edge $e \in \partial K$, $\boldsymbol{n}_{e,K}$ is the unit outward normal vector for K.
- A generic vertex of $\mathcal{V}$ is denoted by v. A given quantity Φ located on v is denoted by $\Phi_{i+1/2,j+1/2}$.

Notations are pictured on Fig. 1.

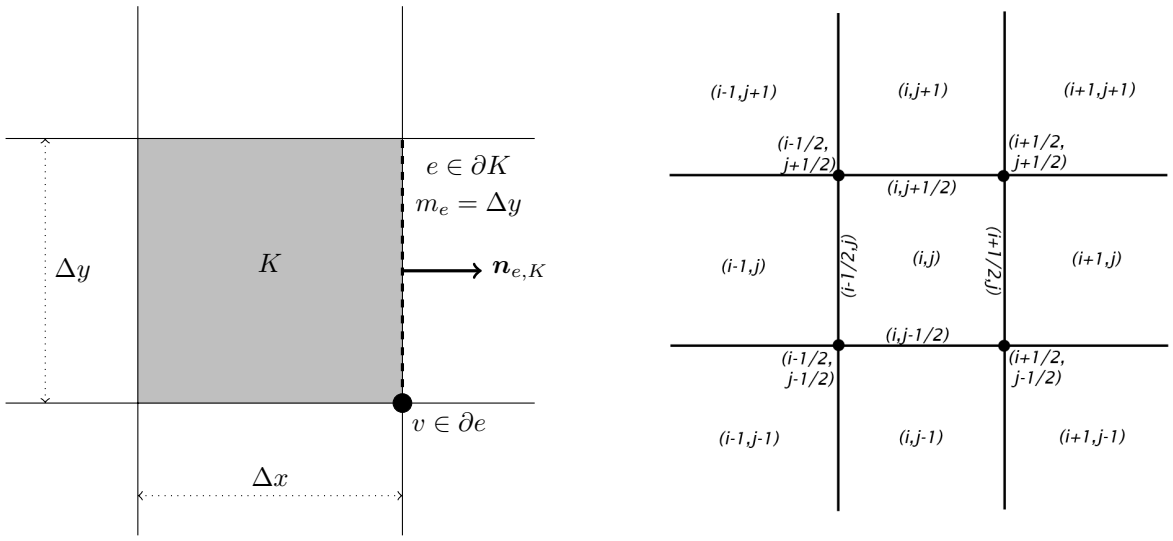

(a) Mesh notations

(b) Variables numbering

Figure 1: Geometric notations

3.2 Discrete operators

Equipped with these geometrical settings, we can now introduce discrete operators that will be needed to construct numerical schemes. Since we only consider colocated numerical schemes, all the unknowns are defined on the cells $K \in \mathcal{K}$. But we will see in the next sections that some other quantities (including the numerical diffusion terms) need to be computed on the edges $e \in \mathcal{E}$ or at the vertices $v \in \mathcal{V}$. Then we need to define discrete operators from cells to edges (and vice-versa) and from cells to vertices (and vice-versa) – see Figure 1. In the following definitions, the notation $X^{\mathcal{B}}_{\mathcal{A}}(\varphi)$ means that the operator X is applied to a quantity φ defined at elements of the set $\mathcal{B}$ and

returns a quantity that is defined at an element of the set $\mathcal{A}$. For example, the first operator below $\nabla_{\mathcal{E}}^{\mathcal{K}}\,\varphi$ is a discrete gradient operator that applies to quantities defined on a cell K and that allows to construct a consistent gradient on an edge e. Discrete gradient and divergence operators are denoted with classic notations. The notation f always denotes an algebraic reconstruction operator. Let us begin with the operators from cells to edges:

$$[\nabla_{\mathcal{E}}^{\mathcal{K}}\,\varphi]_e := -\frac{m_e}{\Delta x\Delta y}\sum_{K\in\mathcal{K}(e)}(\varphi_K\;\boldsymbol{n}_{e,K})\,,$$

$$[f_{\mathcal{E}}^{\mathcal{K}}\,\boldsymbol{\varphi}]_e := \frac{1}{2}\sum_{K\in\mathcal{K}(e)}(\boldsymbol{\varphi}_K\cdot\boldsymbol{n}_{e,K}\;\boldsymbol{n}_{e,K})\,,$$

and from edges to cells:

$$[\nabla_{\mathcal{K}}^{\mathcal{E}}\,\varphi]_K := \frac{1}{m_K}\sum_{e\in\mathcal{E}(K)}(m_e\,\varphi_e\;\boldsymbol{n}_{e,K})\,,$$

$$[\mathrm{div}_{\mathcal{K}}^{\mathcal{E}}\,\boldsymbol{\varphi}]_K := \frac{1}{\Delta x\Delta y}\sum_{e\in\mathcal{E}(K)}(m_e\,\boldsymbol{\varphi}_e\cdot\boldsymbol{n}_{e,K})\,,$$

$$[f_{\mathcal{K}}^{\mathcal{E}}\,\boldsymbol{\varphi}]_K := \frac{1}{2}\sum_{e\in\mathcal{E}(K)}(\boldsymbol{\varphi}_e\cdot\boldsymbol{n}_{e,K}\;\boldsymbol{n}_{e,K})\,,$$

where $\mathcal{K}(e) := \{K\in\mathcal{K}\mid e\in\partial K\}$ the set of adjacent cells to an edge e and $\mathcal{E}(K) := \{e\in\mathcal{E}\mid e\in\partial K\}$ the set of adjacent edges to a cell K.

Remark 3.1. *Let us mention that the $\frac{1}{2}$ coefficient in the definition of $f_{\mathcal{K}}^{\mathcal{E}}$ is not natural as there are 4 edges associated to a given cell. However, it is consistent insofar as we only consider values in normal directions. The same remark holds for $f_{\mathcal{V}}^{\mathcal{E}}$ below.*

Then we define reconstruction operators from edges to vertices (and vice-versa):

$$[f_{\mathcal{V}}^{\mathcal{E}}\,\boldsymbol{\varphi}]_v := \frac{1}{2}\sum_{e\in\mathcal{E}(v)}(\boldsymbol{\varphi}_e\cdot\boldsymbol{n}_e)\,\boldsymbol{n}_e\,,$$

$$[f_{\mathcal{E}}^{\mathcal{V}}\,\varphi]_e := \frac{1}{2}\sum_{v\in\mathcal{V}(e)}\varphi_v\,,$$

$$[f_{\mathcal{E}}^{\mathcal{V}}\,\boldsymbol{\varphi}]_e := \frac{1}{2}\sum_{v\in\mathcal{V}(e)}(\boldsymbol{\varphi}_v\cdot\boldsymbol{n}_e)\,\boldsymbol{n}_e\,,$$

with $\mathcal{E}(v) := \{e\in\mathcal{E}\mid v\in\partial e\}$ the set of adjacent edges to a vertex v, $\mathcal{V}(e) := \{v\in\mathcal{V}\mid v\in\partial e\}$ the set of adjacent vertices to an edge e.
We will also need a divergence operator from edges to vertices:

$$[\mathrm{div}_{\mathcal{V}}^{\mathcal{E}}\,\boldsymbol{\varphi}]_{i+1/2,j+1/2} := \frac{1}{\Delta x}\left(\boldsymbol{\varphi}_{i+1,j+1/2}-\boldsymbol{\varphi}_{i,j+1/2}\right)\cdot\boldsymbol{e}_x + \frac{1}{\Delta y}\left(\boldsymbol{\varphi}_{i+1/2,j+1}-\boldsymbol{\varphi}_{i+1/2,j}\right)\cdot\boldsymbol{e}_y,$$

where $\boldsymbol{e}_x$ (respectively $\boldsymbol{e}_y$) is the unit vector in the direction x (respectively y).
Moreover we define operators from cells to vertices, where we use the notation $\boldsymbol{\varphi} := (\varphi,\psi)$

$$\begin{aligned}
[\nabla_{\mathcal{V}}^{\mathcal{K}}\,\varphi]_{i+1/2,j+1/2} &:= [f_{\mathcal{V}}^{\mathcal{E}}\,\nabla_{\mathcal{E}}^{\mathcal{K}}\,\varphi]_{i+1/2,j+1/2},\\
&= \frac{1}{2}\begin{pmatrix}\dfrac{\varphi_{i+1,j+1}-\varphi_{i,j+1}}{\Delta x}+\dfrac{\varphi_{i+1,j}-\varphi_{i,j}}{\Delta x}\\[2ex] \dfrac{\varphi_{i+1,j+1}-\varphi_{i+1,j}}{\Delta y}+\dfrac{\varphi_{i,j+1}-\varphi_{i,j}}{\Delta y}\end{pmatrix},\\
[\mathrm{div}_{\mathcal{V}}^{\mathcal{K}}\,\boldsymbol{\varphi}]_{i+1/2,j+1/2} &:= \frac{1}{2}\left[\frac{\varphi_{i+1,j+1}-\varphi_{i,j+1}}{\Delta x}+\frac{\varphi_{i+1,j}-\varphi_{i,j}}{\Delta x}\right]+\frac{1}{2}\left[\frac{\psi_{i+1,j+1}-\psi_{i+1,j}}{\Delta y}+\frac{\psi_{i,j+1}-\psi_{i,j}}{\Delta y}\right],\\
[f_{\mathcal{V}}^{\mathcal{K}}\,\boldsymbol{\varphi}]_{i+1/2,j+1/2} &:= [f_{\mathcal{V}}^{\mathcal{E}}\,f_{\mathcal{E}}^{\mathcal{K}}\,\boldsymbol{\varphi}]_{i+1/2,j+1/2},\\
&= \frac{\boldsymbol{\varphi}_{i+1,j+1}+\boldsymbol{\varphi}_{i,j+1}+\boldsymbol{\varphi}_{i+1,j}+\boldsymbol{\varphi}_{i,j}}{4}\,,
\end{aligned}$$

and from vertices to cells:

$$
\begin{aligned}
[\nabla_{\mathcal{K}}^{\mathcal{V}}\,\varphi]_{i,j} &:= [\nabla_{\mathcal{K}}^{\mathcal{E}}\, f_{\mathcal{E}}^{\mathcal{V}}\,\varphi]_{i,j},\\
&= \frac{1}{2}\begin{pmatrix} \dfrac{\varphi_{i+1/2,j+1/2}-\varphi_{i-1/2,j+1/2}}{\Delta x} + \dfrac{\varphi_{i+1/2,j-1/2}-\varphi_{i-1/2,j-1/2}}{\Delta x} \\ \dfrac{\varphi_{i+1/2,j+1/2}-\varphi_{i+1/2,j-1/2}}{\Delta y} + \dfrac{\varphi_{i-1/2,j+1/2}-\varphi_{i-1/2,j-1/2}}{\Delta y} \end{pmatrix},\\
[\mathrm{div}_{\mathcal{K}}^{\mathcal{V}}\,\boldsymbol{\varphi}]_{i,j} &:= [\mathrm{div}_{\mathcal{K}}^{\mathcal{E}}\, f_{\mathcal{E}}^{\mathcal{V}}\,\boldsymbol{\varphi}]_{i,j},\\
&= \frac{1}{2}\left[\frac{\varphi_{i+1/2,j+1/2}-\varphi_{i-1/2,j+1/2}}{\Delta x} + \frac{\varphi_{i+1/2,j-1/2}-\varphi_{i-1/2,j-1/2}}{\Delta x}\right]\\
&\qquad + \frac{1}{2}\left[\frac{\psi_{i+1/2,j+1/2}-\psi_{i+1/2,j-1/2}}{\Delta y} + \frac{\psi_{i-1/2,j+1/2}-\psi_{i-1/2,j-1/2}}{\Delta y}\right],\\
[f_{\mathcal{K}}^{\mathcal{V}}\,\boldsymbol{\varphi}]_{i,j} &:= [f_{\mathcal{K}}^{\mathcal{E}}\, f_{\mathcal{E}}^{\mathcal{V}}\,\boldsymbol{\varphi}]_{i,j},\\
&= \frac{\boldsymbol{\varphi}_{i+1/2,j+1/2}+\boldsymbol{\varphi}_{i-1/2,j+1/2}+\boldsymbol{\varphi}_{i+1/2,j-1/2}+\boldsymbol{\varphi}_{i-1/2,j-1/2}}{4}.
\end{aligned}
$$

Finally we need to define upwind divergence operators that will be used to discretise the transport part of the equations in order to ensure the stability of the numerical schemes. In the following definitions, the quantity

$$\varphi^{\pm} = \frac{1}{2}(\varphi \pm |\varphi|)$$

will refer to the positive and negative parts of any scalar function φ.
From edges to cells, the operator reads

$$\left[\mathbf{div}_{\mathcal{K}}^{\mathcal{E},up}(\boldsymbol{\psi}\otimes\boldsymbol{\varphi})\right]_K := \frac{1}{\Delta x\Delta y}\sum_{e\in\mathcal{E}(K)} m_e\left(\boldsymbol{\psi}_K(\boldsymbol{\varphi}_e\cdot\boldsymbol{n}_{e,K})^+ + \boldsymbol{\psi}_{K_e}(\boldsymbol{\varphi}_e\cdot\boldsymbol{n}_{e,K})^-\right),$$

where K_e is the cell neighbouring e other than K.

3.3 Mimetic properties

These discrete operators satisfy some important properties that will be used to prove stability and accuracy properties for the numerical schemes we propose in the next section. Lemmas 3.3 and 3.4 below can be obtained through a rearrangement of terms in the sum of the scalar products and by neglecting boundary terms. Some of the most complex properties have been proven by computer algebra system.

Lemma 3.2. *We first mention some local properties about the permutation of the derivative, reconstruction and orthogonal operators.*

i) $[f_{\mathcal{V}}^{\mathcal{K}}(\boldsymbol{\varphi}^{\perp})]_v = ([f_{\mathcal{V}}^{\mathcal{K}}\,\boldsymbol{\varphi}]_v)^{\perp}$

ii) $\left[\mathrm{div}_{\mathcal{V}}^{\mathcal{E}}\left((f_{\mathcal{E}}^{\mathcal{K}}(\boldsymbol{\varphi}^{\perp}))^{\perp}\right)\right]_v = -\left[\mathrm{div}_{\mathcal{V}}^{\mathcal{K}}\,\boldsymbol{\varphi}\right]_v$

iii) $\left[\mathrm{div}_{\mathcal{K}}^{\mathcal{V}}\, f_{\mathcal{V}}^{\mathcal{K}}\,\boldsymbol{\varphi}\right]_K = \left[f_{\mathcal{K}}^{\mathcal{V}}\,\mathrm{div}_{\mathcal{V}}^{\mathcal{K}}\,\boldsymbol{\varphi}\right]_K$

iv) $\left[\mathrm{div}_{\mathcal{V}}^{\mathcal{E}}\left((\nabla_{\mathcal{E}}^{\mathcal{K}}\,\varphi)^{\perp}\right)\right]_v = 0$

We now define the four scalar products

$$\langle\varphi,\psi\rangle_{\mathcal{K}} = \sum_{K\in\mathcal{K}}\varphi_K\,\psi_K, \qquad \langle\boldsymbol{\varphi},\boldsymbol{\psi}\rangle_{\mathcal{K}} = \sum_{K\in\mathcal{K}}\boldsymbol{\varphi}_K\cdot\boldsymbol{\psi}_K, \qquad \langle\boldsymbol{\varphi},\boldsymbol{\psi}\rangle_{\mathcal{V}} = \sum_{v\in\mathcal{V}}\boldsymbol{\varphi}_v\cdot\boldsymbol{\psi}_v \qquad \text{and} \qquad \langle\boldsymbol{\varphi},\boldsymbol{\psi}\rangle_{\mathcal{E}} = \sum_{e\in\mathcal{E}}\boldsymbol{\varphi}_e\cdot\boldsymbol{\psi}_e.$$

Lemma 3.3. *Neglecting boundary terms, we have the following properties for the reconstruction and orthogonal operators*

i) $\left\langle\boldsymbol{\varphi},(f_{\mathcal{K}}^{\mathcal{E}}\,\boldsymbol{\psi})^{\perp}\right\rangle_{\mathcal{K}} = -\left\langle f_{\mathcal{E}}^{\mathcal{K}}(\boldsymbol{\varphi}^{\perp}),\boldsymbol{\psi}\right\rangle_{\mathcal{E}}$

ii) $\left\langle f_{\mathcal{K}}^{\mathcal{V}}\, f_{\mathcal{V}}^{\mathcal{K}}(\boldsymbol{\psi}^{\perp}), \boldsymbol{\psi}\right\rangle_{\mathcal{K}} = 0$

iii) $\left\langle \left[f_{\mathcal{K}}^{\mathcal{V}}\left((f_{\mathcal{V}}^{\mathcal{K}}\,\varphi)(f_{\mathcal{V}}^{\mathcal{K}}\,\boldsymbol{\psi})\right)\right]^{\perp}, \boldsymbol{\psi}\right\rangle_{\mathcal{K}} = 0$

Lemma 3.4. *Neglecting boundary terms, we have the following mimetic properties for the discrete gradient and divergence operators, including for some of them the reconstruction operators*

i) $\left\langle \varphi, \mathrm{div}_{\mathcal{K}}^{\mathcal{E}}\,\boldsymbol{\psi}\right\rangle_{\mathcal{K}} = -\left\langle \nabla_{\mathcal{E}}^{\mathcal{K}}\,\varphi, \boldsymbol{\psi}\right\rangle_{\mathcal{E}}$

ii) $\left\langle \varphi, \mathrm{div}_{\mathcal{V}}^{\mathcal{K}}\,\boldsymbol{\psi}\right\rangle_{\mathcal{V}} = -\left\langle \nabla_{\mathcal{K}}^{\mathcal{V}}\,\varphi, \boldsymbol{\psi}\right\rangle_{\mathcal{K}}$

iii) $\left\langle f_{\mathcal{K}}^{\mathcal{E}}\,\nabla_{\mathcal{E}}^{\mathcal{K}}\,\varphi, \boldsymbol{\psi}\right\rangle_{\mathcal{K}} = -\left\langle \varphi, \mathrm{div}_{\mathcal{K}}^{\mathcal{E}}\, f_{\mathcal{E}}^{\mathcal{K}}\,\boldsymbol{\psi}\right\rangle_{\mathcal{K}}$

iv) $\left\langle f_{\mathcal{K}}^{\mathcal{V}}\,\nabla_{\mathcal{V}}^{\mathcal{K}}\,\varphi, \boldsymbol{\psi}\right\rangle_{\mathcal{K}} = -\left\langle \varphi, f_{\mathcal{K}}^{\mathcal{V}}\,\mathrm{div}_{\mathcal{V}}^{\mathcal{K}}\,\boldsymbol{\psi}\right\rangle_{\mathcal{K}}$

v) $\left\langle f_{\mathcal{K}}^{\mathcal{V}}\left((f_{\mathcal{V}}^{\mathcal{K}}\,\varphi)(\nabla_{\mathcal{V}}^{\mathcal{K}}\,\Phi)\right), \boldsymbol{\psi}\right\rangle_{\mathcal{K}} = -\left\langle \Phi, \mathrm{div}_{\mathcal{K}}^{\mathcal{V}}\left((f_{\mathcal{V}}^{\mathcal{K}}\,\varphi)(f_{\mathcal{V}}^{\mathcal{K}}\,\boldsymbol{\psi})\right)\right\rangle_{\mathcal{K}}$

4 Well-balanced and stable finite-volume scheme

When considering hyperbolic equations, classic finite-volume schemes in colocated two-dimensional cartesian framework are often 5-point schemes. Indeed the update of the quantities of interest in a cell K of the tessellation $\mathcal{K}$ requires the computation of the fluxes through the four edges of its boundary ∂K, see Figure 1. For a first order scheme, the numerical flux through an edge $e \in \mathcal{E}$ is generally computed from the values of the quantities in the two neighbouring cells. Hence, the update of the quantities in a cell K involves five cells of the tessellation $\mathcal{K}$. We refer to [16, 24] for more details about classic first order finite-volume schemes for hyperbolic problems.
In the last section of the paper, devoted to the numerical tests, such a 5-point scheme, typically the HLLC scheme, see [24], will be considered as a standard scheme to which we will compare the schemes we design in the next sections. Because of the fundamentally two-dimensional character of the geostrophic equilibrium, these schemes induce a larger stencil. Note that to consider larger stencils is also a common way to design high order schemes in a finite-volume framework through the MUSCL strategy, see [16,24], and is also commonly used in diffusion problems since the computation of numerical fluxes needs the reconstruction of a complete two-dimensional gradient, see [12]. In this section, we present two 9-point numerical schemes for the shallow water equations with Coriolis source term, based on a discretisation of the geostrophic equilibrium (3) on the edges.

4.1 Classic Godunov-type scheme

HLLC is the standard scheme for homogeneous 2D Shallow water equations [24] (chapters 10.4 p.322 and 10.6 p.331) based on a particular choice of wave speeds (relation 10.48 p.328). This scheme can be rewritten with the operators defined in section 3.2 as:

$$\frac{\mathrm{d}}{\mathrm{dt}} W_{\alpha,K} + \left[\mathrm{div}_{\mathcal{K}}^{\mathcal{E}}\,\boldsymbol{\mathcal{F}}_{\alpha}^{hllc}\right]_K + S_{\alpha,K} = 0, \quad \alpha \in \{1,2,3\} \tag{6}$$

with $\boldsymbol{W}_K := (h_K,\, h_K \boldsymbol{u}_K)^T$, $\boldsymbol{S}_K := (0,\, \omega h_K \boldsymbol{u}_K^{\perp})^T$ and where $\boldsymbol{\mathcal{F}}^{hllc}$ is the classic HLLC numerical flux. In [6, §2.4.6] it is proven that with a suitable choice of wave speeds this scheme satisfies a discrete entropy inequality. As it will be shown in Section 5 its linearised version does not preserve the geostrophic equilibrium (3).

4.2 Solely entropic (SE) scheme

In [2], we proposed a first numerical scheme for which we proved a semi-discrete counterpart of (5). However, we also exhibited that the linearised version of the scheme failed to preserve the geostrophic balance, which does not prevent in practice from providing better numerical results for all the test cases we had performed compared to classic numerical schemes. Let us recall this scheme following the discrete operators introduced in Section 3.2 in order to compare with the new scheme in terms of formulation, properties and numerical results.

This scheme reads:

$$\begin{cases} \dfrac{\mathrm{d}}{\mathrm{d}t} h_K + \left[\mathrm{div}_{\mathcal{K}}^{\mathcal{E}} \boldsymbol{\mathcal{F}}^{SE} \right]_K = 0, \\ \dfrac{\mathrm{d}}{\mathrm{d}t} (h_K \boldsymbol{u}_K) + \left[\mathbf{div}_{\mathcal{K}}^{\mathcal{E},up} (\boldsymbol{u} \otimes \boldsymbol{\mathcal{F}}^{SE}) \right]_K + h_K \, \left[f_{\mathcal{K}}^{\mathcal{E}} \nabla_{\mathcal{E}}^{\mathcal{K}} \phi \right]_K - \left[\nabla_{\mathcal{K}}^{\mathcal{V}} \pi \right]_K = -\omega \left(h_K \boldsymbol{u}_K - \left[f_{\mathcal{K}}^{\mathcal{E}} \boldsymbol{q} \right]_K \right)^{\perp}, \end{cases} \tag{7}$$

where the mass fluxes are defined at the level of the edge e as:

$$\boldsymbol{\mathcal{F}}_e^{SE} = \left[f_{\mathcal{E}}^{\mathcal{K}} (h\boldsymbol{u}) \right]_e - \boldsymbol{q}_e \,, \tag{8}$$

with the numerical diffusion term on the flow rate

$$\boldsymbol{q}_e = \gamma \, \frac{\Lambda}{g} \max\{\Delta x, \Delta y\} \left[\omega \, f_{\mathcal{E}}^{\mathcal{K}} (\boldsymbol{u}^{\perp}) + \nabla_{\mathcal{E}}^{\mathcal{K}} \phi \right]_e , \tag{9}$$

while the numerical diffusion term on the hydrostatic pressure is defined at the vertices

$$\pi_v = \nu \Lambda \, \max\{\Delta x, \Delta y\} \left[f_{\mathcal{V}}^{\mathcal{K}} h \right]_v \left[\mathrm{div}_{\mathcal{V}}^{\mathcal{K}} \boldsymbol{u} \right]_v . \tag{10}$$

Notice that the expressions chosen for $\boldsymbol{q}_e$ and π_v are consistent with the choice inferred from the continuous analysis – see Section 2. Let us also mention that Scheme (7) is a 9-point scheme due to the term $\nabla_{\mathcal{K}}^{\mathcal{V}} \pi$.
Finally, a classic choice is to take (see [6], section 2.4.2):

$$\Lambda = \max_{K \in \mathcal{K}} \left\{ \|\boldsymbol{u}_K\| + \sqrt{g h_K} \right\}. \tag{11}$$

Let us mention that ν and γ are dimensionless constants.

Decreasing of the semi-discrete energy: A discrete counterpart of (5) can be proven for this scheme [2] with a similar proof to Proposition 4.4 below.

Linearised well-balanced property: If we assume the geostrophic equilibrium on edges holds, *i.e.* $\omega \left[f_{\mathcal{E}}^{\mathcal{K}} (\boldsymbol{u}^{\perp}) \right]_e + \left[\nabla_{\mathcal{E}}^{\mathcal{K}} \phi \right]_e = 0$, it implies that $\boldsymbol{q}_e = 0$ and $\pi_v = 0$ but, since $\left[f_{\mathcal{K}}^{\mathcal{E}} (f_{\mathcal{E}}^{\mathcal{K}} (\boldsymbol{u}^{\perp})) \right]_K \neq \boldsymbol{u}_K^{\perp}$, the geostrophic term $\omega \, \boldsymbol{u}_K^{\perp} + \left[f_{\mathcal{K}}^{\mathcal{E}} \nabla_{\mathcal{E}}^{\mathcal{K}} \phi \right]_K$ that appears in the update of the momentum in (7) does not vanish. Conversely, if $\omega \, \boldsymbol{u}_K^{\perp} + \left[f_{\mathcal{K}}^{\mathcal{E}} \nabla_{\mathcal{E}}^{\mathcal{K}} \phi \right]_K = 0$, for the same reasons, $\boldsymbol{q}_e \neq 0$. Hence, the scheme is not able to preserve any discrete geostrophic equilibrium.

4.3 Entropic well-balanced (EWB) scheme

In this part, let us present a new 9-point scheme which satisfies both aforementioned properties, namely a non-increasing semi-discrete energy and a linearised well-balanced property. To do so, we observed that a geostrophic equilibrium on the edges implies a geostrophic equilibrium at the vertices. This remark helped us to derive suitable consistent approximations of the remaining terms in the momentum equation (located on the cells).
For the sake of simplicity, we first present a non-conservative formulation that is the closest to the previous scheme before presenting the conservative version.

4.3.1 Non-conservative semi-discrete formulation

$$\begin{cases} \dfrac{\mathrm{d}}{\mathrm{d}t} h_K + \left[\mathrm{div}_{\mathcal{K}}^{\mathcal{E}} \boldsymbol{\mathcal{F}}^{EWB} \right]_K = 0, \\ \dfrac{\mathrm{d}}{\mathrm{d}t} (h_K \boldsymbol{u}_K) + \left[\mathbf{div}_{\mathcal{K}}^{\mathcal{E},up} (\boldsymbol{u} \otimes \boldsymbol{\mathcal{F}}^{EWB}) \right]_K + h_K \left[f_{\mathcal{K}}^{\mathcal{V}} \nabla_{\mathcal{V}}^{\mathcal{K}} \phi \right]_K - \left[\nabla_{\mathcal{K}}^{\mathcal{V}} \pi \right]_K \\ \qquad\qquad = -\omega \left(h_K \left[f_{\mathcal{K}}^{\mathcal{V}} f_{\mathcal{V}}^{\mathcal{K}} \boldsymbol{u} \right]_K - \left[f_{\mathcal{K}}^{\mathcal{E}} \boldsymbol{q} \right]_K \right)^{\perp}, \end{cases} \tag{12}$$

where the interface fluxes are defined at the level of the edge e as:

$$\boldsymbol{\mathcal{F}}_e^{EWB} = \left[f_{\mathcal{E}}^{\mathcal{V}} f_{\mathcal{V}}^{\mathcal{K}} (h\boldsymbol{u}) \right]_e - \boldsymbol{q}_e \,. \tag{13}$$

The numerical diffusion term on the flow rate $\boldsymbol{q}_e$ is still defined by (9) and the numerical diffusion term on the hydrostatic pressure π_v by (10)

Remark 4.1. *Most of finite-volume schemes have a 2-point flux, like $\mathcal{F}^{SE}$ (8) for the solely entropic scheme or the classic HLLC flux $\mathcal{F}^{hllc}$. However, $\mathcal{F}^{EWB}$ and $\mathcal{F}^{C}$ (22) for the conservative formulation are 6-point fluxes due to the reconstruction on vertices.*

Semi-discrete energy: We first show that Scheme (12) ensures a discrete counterpart of (5) through semi-discrete mechanic energy estimates. We need the two following lemmas, describing the evolution of potential and kinetic energies.

Lemma 4.2 (Potential energy)**.** *We set* $E_K^p = \frac{1}{2} g\,(h_K)^2$ *for* $K \in \mathcal{K}$*. Then:*

$$\frac{\mathrm{d}}{\mathrm{d}t} E_K^p + \phi_K \left[\mathrm{div}_{\mathcal{K}}^{\mathcal{V}} f_{\mathcal{V}}^{\mathcal{K}}(h\boldsymbol{u})\right]_K - \phi_K \,\mathrm{div}_{\mathcal{K}}^{\mathcal{E}} \boldsymbol{q} = 0. \tag{14}$$

Proof. Multiply the first equation of (12) by ϕ_K and use the definition of operator $\mathrm{div}_{\mathcal{K}}^{\mathcal{V}}$. □

Lemma 4.3 (Kinetic energy)**.** *We set* $E_K^k = \frac{1}{2} h_K \|\boldsymbol{u}_K\|^2$ *for* $K \in \mathcal{K}$*. Then:*

$$\begin{aligned}\frac{\mathrm{d}}{\mathrm{d}t} E_K^k + \left[\mathbf{div}_{\mathcal{K}}^{\mathcal{E},up}\left(\frac{\|\boldsymbol{u}\|^2}{2}\boldsymbol{\mathcal{F}}^{EWB}\right)\right]_K + h_K \boldsymbol{u}_K \cdot \left[f_{\mathcal{K}}^{\mathcal{V}} \nabla_{\mathcal{V}}^{\mathcal{K}} \phi\right]_K \\ \leq -\omega\left(h_K \boldsymbol{u}_K \cdot \left[f_{\mathcal{K}}^{\mathcal{V}} f_{\mathcal{V}}^{\mathcal{K}}(\boldsymbol{u}^\perp)\right]_K - \boldsymbol{u}_K \cdot \left(\left[f_{\mathcal{K}}^{\mathcal{E}} \boldsymbol{q}\right]_K\right)^\perp\right) + \boldsymbol{u}_K \cdot \left[\nabla_{\mathcal{K}}^{\mathcal{V}} \pi\right]_K.\end{aligned} \tag{15}$$

Proof. Using the first equation of (12) we write:

$$\begin{aligned}\frac{\mathrm{d}}{\mathrm{d}t}\left(\frac{1}{2} h_K \|\boldsymbol{u}_K\|^2\right) &= \boldsymbol{u}_K \cdot \frac{\mathrm{d}}{\mathrm{d}t}(h_K \boldsymbol{u}_K) - \frac{1}{2}\|\boldsymbol{u}_K\|^2 \frac{\mathrm{d}}{\mathrm{d}t} h_K \\ &= -h_K \boldsymbol{u}_K \cdot \left[f_{\mathcal{K}}^{\mathcal{V}} \nabla_{\mathcal{V}}^{\mathcal{K}} \phi\right]_K - \boldsymbol{u}_K \cdot \left[\mathbf{div}_{\mathcal{K}}^{\mathcal{E},up}(\boldsymbol{u} \otimes \boldsymbol{\mathcal{F}}^{EWB})\right]_K + \omega \boldsymbol{u}_K \cdot \left(\left[f_{\mathcal{K}}^{\mathcal{E}} \boldsymbol{q}\right]_K\right)^\perp \\ &\quad + \frac{1}{2}\|\boldsymbol{u}_K\|^2 \left[\mathrm{div}_{\mathcal{K}}^{\mathcal{E}} \boldsymbol{\mathcal{F}}^{EWB}\right]_K + \boldsymbol{u}_K \cdot \left[\nabla_{\mathcal{K}}^{\mathcal{V}} \pi\right]_K - \omega h_K \boldsymbol{u}_K \left[f_{\mathcal{K}}^{\mathcal{V}} f_{\mathcal{V}}^{\mathcal{K}}(\boldsymbol{u}^\perp)\right]_K.\end{aligned}$$

After some basic computations, we get the relations

$$\begin{aligned}&\frac{1}{2}\|\boldsymbol{u}_K\|^2 \left[\mathrm{div}_{\mathcal{K}}^{\mathcal{E}} \boldsymbol{\mathcal{F}}^{EWB}\right]_K - \boldsymbol{u}_K \cdot \left[\mathbf{div}_{\mathcal{K}}^{\mathcal{E},up}\left(\boldsymbol{u} \otimes \boldsymbol{\mathcal{F}}^{EWB}\right)\right]_K \\ &\qquad = -\left[\mathbf{div}_{\mathcal{K}}^{\mathcal{E},up}\left(\frac{\|\boldsymbol{u}_K\|^2}{2}\boldsymbol{\mathcal{F}}^{EWB}\right)\right]_K + \frac{1}{2\Delta x \Delta y} \sum_{e \subset \partial K} \left(m_e \|\boldsymbol{u}_K - \boldsymbol{u}_{K_e}\|^2 \left(\boldsymbol{\mathcal{F}}_e^{EWB} \cdot \boldsymbol{n}_{e,K}\right)^-\right).\end{aligned}$$

The second term of the right hand side being non-positive, we get the announced result . □

Proposition 4.4 (Decreasing of the semi-discrete energy)**.** *We define the total energy* $E_K = E_K^p + E_K^k$*. Then we obtain a discrete counterpart of* (5)

$$\begin{aligned}&\frac{\mathrm{d}}{\mathrm{d}t}\left(\sum_{K \in \mathbb{T}} \Delta x \Delta y E_K\right) \\ &\quad \leq -\Delta x \Delta y \max\{\Delta x, \Delta y\}\left(\sum_{v \in \mathbb{V}}\left(\nu\Lambda \left[f_{\mathcal{V}}^{\mathcal{K}} h\right]_v \left(\left[\mathrm{div}_{\mathcal{V}}^{\mathcal{K}} \boldsymbol{u}\right]_v\right)^2\right) + \sum_{e \in \mathbb{E}}\left(\gamma \frac{\Lambda}{g}\|\omega \left[f_{\mathcal{E}}^{\mathcal{K}}(\boldsymbol{u}^\perp)\right]_e + \left[\nabla_{\mathcal{E}}^{\mathcal{K}} \phi\right]_e\|^2\right)\right).\end{aligned} \tag{16}$$

Proof. Gathering both relations (14) and (15), we obtain the following estimate for the total energy $E_K = E_K^p + E_K^k$:

$$\begin{aligned}&\frac{\mathrm{d}}{\mathrm{d}t} E_K + \left[\mathbf{div}_{\mathcal{K}}^{\mathcal{E},up}\left(\frac{\|\boldsymbol{u}\|^2}{2}\boldsymbol{\mathcal{F}}^{EWB}\right)\right]_K + \phi_K \left[\mathrm{div}_{\mathcal{K}}^{\mathcal{V}} f_{\mathcal{V}}^{\mathcal{K}}(h\boldsymbol{u})\right]_K + h_K \boldsymbol{u}_K \cdot \left[f_{\mathcal{K}}^{\mathcal{V}} \nabla_{\mathcal{V}}^{\mathcal{K}} \phi\right]_K \\ &\qquad \leq -\omega\left(h_K \boldsymbol{u}_K \cdot \left[f_{\mathcal{K}}^{\mathcal{V}} f_{\mathcal{V}}^{\mathcal{K}}(\boldsymbol{u}^\perp)\right]_K - \boldsymbol{u}_K \cdot \left(\left[f_{\mathcal{K}}^{\mathcal{E}} \boldsymbol{q}_{\mathcal{E}}\right]_K\right)^\perp\right) + \phi_K \left[\mathrm{div}_{\mathcal{K}}^{\mathcal{E}} \boldsymbol{q}\right]_K + \boldsymbol{u}_K \cdot \left[\nabla_{\mathcal{K}}^{\mathcal{V}} \pi\right]_K.\end{aligned}$$

By telescoping and using periodic boundary conditions we get:

$$\sum_{K \in \mathbb{T}} \left[\mathbf{div}_{\mathcal{K}}^{\mathcal{E},up}\left(\|\boldsymbol{u}\|^2 \boldsymbol{\mathcal{F}}^{EWB}\right)\right]_K = 0.$$

Using iii) of Lemma 3.2 and iv) of Lemma 3.4, we get:

$$\sum_{K\in\mathbb{T}} \left(\phi_K \left[\mathrm{div}_{\mathcal{K}}^{\mathcal{V}} f_{\mathcal{V}}^{\mathcal{K}}(h\boldsymbol{u}) \right]_K + h_K \boldsymbol{u}_K \cdot \left[f_{\mathcal{K}}^{\mathcal{V}} \nabla_{\mathcal{V}}^{\mathcal{K}} \phi \right]_K \right) = 0. \tag{17}$$

Thanks to ii) of Lemma 3.3 we get:

$$\sum_{K\in\mathbb{T}} \left[h_K \boldsymbol{u}_K \cdot \left[f_{\mathcal{K}}^{\mathcal{V}} f_{\mathcal{V}}^{\mathcal{K}}(\boldsymbol{u}^\perp) \right]_K \right] = 0.$$

Finally, i) and ii) of Lemma 3.4 and i) of Lemma 3.3 leads us to the following semi-discrete inequality:

$$\frac{\mathrm{d}}{\mathrm{dt}} \left(\sum_{K\in\mathbb{T}} \Delta x \Delta y E_K \right) \leq -\Delta x \Delta y \left(\sum_{v\in\mathbb{V}} \left(\pi_v \left[\mathrm{div}_{\mathcal{V}}^{\mathcal{K}} \boldsymbol{u} \right]_v \right) + \sum_{e\in\mathbb{E}} \left(\boldsymbol{q}_e \cdot \left(\omega \left[f_{\mathcal{E}}^{\mathcal{K}}(\boldsymbol{u}^\perp) \right]_e + \left[\nabla_{\mathcal{E}}^{\mathcal{K}} \phi \right]_e \right) \right) \right).$$

With the choices (9) and (10), we finally obtain the result. □

Linearised well-balanced property: The linearised version of Scheme (12) around $(h_0, \mathbf{0})$ is the following:

$$\begin{cases} \dfrac{\mathrm{d}}{\mathrm{dt}} h_K + h_0 \left[\mathrm{div}_{\mathcal{K}}^{\mathcal{V}} f_{\mathcal{V}}^{\mathcal{K}} \boldsymbol{u} \right]_K - h_0 \left[\mathrm{div}_{\mathcal{K}}^{\mathcal{E}} \tilde{\boldsymbol{q}} \right]_K = 0, \\ \dfrac{\mathrm{d}}{\mathrm{dt}} \boldsymbol{u}_K + \left[f_{\mathcal{K}}^{\mathcal{V}} \nabla_{\mathcal{V}}^{\mathcal{K}} \phi \right]_K - \left[\nabla_{\mathcal{K}}^{\mathcal{V}} \tilde{\pi} \right]_K = -\omega \left(\left[f_{\mathcal{K}}^{\mathcal{V}} f_{\mathcal{V}}^{\mathcal{K}} \boldsymbol{u} \right]_K - \left[f_{\mathcal{K}}^{\mathcal{E}} \tilde{\boldsymbol{q}} \right]_K \right)^\perp, \end{cases} \tag{18}$$

where

$$\tilde{\boldsymbol{q}}_e = \gamma \frac{\Lambda}{g h_0} \max\{\Delta x, \Delta y\} \left(\omega \left[f_{\mathcal{E}}^{\mathcal{K}}(\boldsymbol{u}^\perp) \right]_e + \left[\nabla_{\mathcal{E}}^{\mathcal{K}} \phi \right]_e \right) \quad \text{and} \quad \tilde{\pi}_v = \nu \Lambda \max\{\Delta x, \Delta y\} \left[\mathrm{div}_{\mathcal{V}}^{\mathcal{K}} \boldsymbol{u} \right]_v.$$

Proposition 4.5. *Any field $(\phi, \boldsymbol{u})_K$ satisfying the discrete geostrophic equilibrium on edges $\omega \left[f_{\mathcal{E}}^{\mathcal{K}}(\boldsymbol{u}^\perp) \right]_e + \left[\nabla_{\mathcal{E}}^{\mathcal{K}} \phi \right]_e = 0$ is a steady solution of the linearised scheme* (18).

Proof. Let us assume that

$$\omega \left[f_{\mathcal{E}}^{\mathcal{K}}(\boldsymbol{u}^\perp) \right]_e + \left[\nabla_{\mathcal{E}}^{\mathcal{K}} \phi \right]_e = \mathbf{0} \tag{19}$$

and hence $\tilde{\boldsymbol{q}}_e = \mathbf{0}$. Then:

$$\begin{aligned} \text{Lemma 3.2, ii)} \implies \quad & \mathrm{div}_{\mathcal{V}}^{\mathcal{K}} \boldsymbol{u} = -\mathrm{div}_{\mathcal{V}}^{\mathcal{E}}((f_{\mathcal{E}}^{\mathcal{K}}(\boldsymbol{u}^\perp))^\perp) \\ (19) \implies \quad & = \mathrm{div}_{\mathcal{V}}^{\mathcal{E}} \left(\frac{(\nabla_{\mathcal{E}}^{\mathcal{K}} \phi)^\perp}{\omega} \right) \\ \text{Lemma 3.2, iv)} \implies \quad & = 0, \end{aligned} \tag{20}$$

and hence $\tilde{\pi}_v = 0$. Moreover, by definition of operators – see Section 3.2, we have:

$$\omega f_{\mathcal{V}}^{\mathcal{K}}(\boldsymbol{u}^\perp) + \nabla_{\mathcal{V}}^{\mathcal{K}} \phi = f_{\mathcal{V}}^{\mathcal{E}} \left(\omega f_{\mathcal{E}}^{\mathcal{K}}(\boldsymbol{u}^\perp) + \nabla_{\mathcal{E}}^{\mathcal{K}} \phi \right).$$

Hence $\partial_t \boldsymbol{u}_K = 0$.
Moreover, using iii) of Lemma 3.2, we get $\mathrm{div}_{\mathcal{K}}^{\mathcal{V}} f_{\mathcal{V}}^{\mathcal{K}} \boldsymbol{u} = f_{\mathcal{K}}^{\mathcal{V}} \mathrm{div}_{\mathcal{V}}^{\mathcal{K}} \boldsymbol{u} = 0$ due to (20). This implies that $\partial_t h_K = 0$. □

Remark 4.6. *As it contains a reconstruction operator on the velocity, the discrete geostrophic equilibrium $\tilde{\boldsymbol{q}}_e = 0$ also contains spurious solutions*

$$\forall (i,j), \quad \phi_{i,j} = cst \quad \textit{and} \quad \boldsymbol{u}_{i,j} = \left((-1)^i \, a_j, (-1)^j \, b_i \right)^T.$$

4.3.2 Conservative semi-discrete formulation

Here we propose a conservative form of the scheme (12), *i.e.* a version of the scheme with a conservative discrete pressure term as it should be in a finite-volume framework. With the discrete operators introduced in Section 3, the conservative semi-discrete scheme reads:

$$\begin{cases} \dfrac{\mathrm{d}}{\mathrm{dt}} h_K + \left[\mathrm{div}_{\mathcal{K}}^{\mathcal{E}} \boldsymbol{\mathcal{F}}^C\right]_K = 0, \\ \dfrac{\mathrm{d}}{\mathrm{dt}}(h_K \boldsymbol{u}_K) + \left[\mathbf{div}_{\mathcal{K}}^{\mathcal{E},up}(\boldsymbol{u} \otimes \boldsymbol{\mathcal{F}}^C)\right]_K + \left[\nabla_{\mathcal{K}}^{\mathcal{E}} \mathcal{P}\right]_K - \left[\nabla_{\mathcal{K}}^{\mathcal{E}}(f_{\mathcal{E}}^{\mathcal{V}} \pi)\right]_K = -\omega \left[f_{\mathcal{K}}^{\mathcal{E}} \mathcal{F}^C\right]_K^{\perp}, \end{cases} \tag{21}$$

where the interface fluxes are defined at the level of the edges e as:

$$\boldsymbol{\mathcal{F}}_e^C = \left[f_{\mathcal{E}}^{\mathcal{V}} \left((f_{\mathcal{V}}^{\mathcal{K}} h)(f_{\mathcal{V}}^{\mathcal{K}} \boldsymbol{u})\right)\right]_e - \boldsymbol{q}_e \,, \tag{22}$$

the interface pressure as:

$$\mathcal{P}_{i+1/2,j} = \frac{\mathcal{P}_{i+1,j}^x + \mathcal{P}_{i,j}^x}{2}, \qquad \mathcal{P}_{i,j}^x = \frac{g}{2} \times \frac{1}{2}\left[\left(\frac{h_{i,j+1} + h_{i,j}}{2}\right)^2 + \left(\frac{h_{i,j} + h_{i,j-1}}{2}\right)^2\right],$$
$$\mathcal{P}_{i,j+1/2} = \frac{\mathcal{P}_{i,j+1}^y + \mathcal{P}_{i,j}^y}{2}, \qquad \mathcal{P}_{i,j}^y = \frac{g}{2} \times \frac{1}{2}\left[\left(\frac{h_{i+1,j} + h_{i,j}}{2}\right)^2 + \left(\frac{h_{i,j} + h_{i-1,j}}{2}\right)^2\right],$$

and the numerical diffusion terms $\boldsymbol{q}_e$ and π_v are defined by (9) and (10). Note the change on the pressure term has for consequence a change on the mass flux and on the Coriolis term in order to preserve the energy balance.

Proposition 4.7 (Decreasing of the semi-discrete energy)**.** *Scheme* (21) *satisfies a discrete counterpart of* (5) *which is the same as Scheme* (12) *(cf. Proposition 4.4).*

Proof. The proof has the same structure as the one of Proposition 4.4. We first recall that $\mathrm{div}_{\mathcal{K}}^{\mathcal{V}} := \mathrm{div}_{\mathcal{K}}^{\mathcal{E}} f_{\mathcal{E}}^{\mathcal{V}}$. Then, using property iii) of Lemma 3.3 we prove that the Coriolis term does not appear in energy balance. Finally, using the equality

$$\left[\nabla_{\mathcal{K}}^{\mathcal{E}} \mathcal{P}\right]_K = \left[f_{\mathcal{K}}^{\mathcal{V}} \left((f_{\mathcal{V}}^{\mathcal{K}} h)(\nabla_{\mathcal{V}}^{\mathcal{K}} \phi)\right)\right]_K$$

and property v) of Lemma 3.4, we prove an equivalent of Equation (17) which characterises the duality between the flux divergence in the mass equation and the pressure gradient in momentum equation. □

Linearised well-balanced property: The linearised version of the conservative scheme (21) is the same as the non-conservative scheme (12). Hence, we obtain the same results: when the discrete geostrophic equilibrium holds at the vertices, the corrections $\tilde{\boldsymbol{q}}_e$ and $\tilde{\pi}_v$ equal zero and the geostrophic balance expressed on edges is included in the kernel of the numerical scheme.

4.4 Time discretisation

For the discretisation in time, fluxes are taken explicit. Nevertheless it is well known – see [8, 26] – that the forward Euler scheme for the Coriolis term leads in that case to unstable schemes. We thus consider the following semi-implicit discretisation of the Coriolis term for all the presented schemes:

$$\frac{u_x^{n+1} - u_x^n}{\Delta t} = \omega(\theta_x u_y^n + (1-\theta_x) u_y^{n+1}), \qquad \frac{u_y^{n+1} - u_y^n}{\Delta t} = -\omega(\theta_y u_x^n + (1-\theta_y) u_x^{n+1}),$$

with $\theta_x + \theta_y \leq 1$. Here we choose $\theta_x = 1$ and $\theta_y = 0$ so that the system is solved explicitly. The time step is chosen following [1] such that

$$\Delta t^n \leq \min\left\{\frac{2}{\omega}, \frac{\min(\Delta x, \Delta y)}{\Lambda^n}\right\},$$

where Λ^n is the time discretisation of (11).

5 Numerical results

In the following, we present different test cases to highlight the behaviour of the solely entropic scheme (7) and the entropic well-balanced scheme (12), compared to the classic HLLC scheme (6). We study the water depth h and the velocity field $\boldsymbol{u} = (u, v)$, as well as the evolution of the discrete energy. The numerical tests are performed with normalised values for the gravitational constant $g = 1$ and the angular velocity $\omega = 1$. The mesh is defined by a $[101 \times 101]$ Cartesian grid and the numerical diffusion coefficients are set to $\gamma = \nu = 0.5$ (except for the circular dam break test case).

5.1 1D equilibrium

This test case is the counterpart of the lake-at-rest for the classic shallow water equations. It consists in a stationary flow through a channel, with no-slip wall-type boundary conditions at $x = -0.5$ and $x = 0.5$ and periodic boundary conditions at $y = -0.5$ and $y = 0.5$. The initial condition (see Figure 2) is as follows:

$$\boldsymbol{u} = \begin{pmatrix} 0 \\ \epsilon/\omega \end{pmatrix} \quad \text{and} \quad \nabla h = \begin{pmatrix} \epsilon/g \\ 0 \end{pmatrix}, \tag{23}$$

with $\epsilon = 0.01$.
Hence, this initial condition is both a stationary solution of the nonlinear Shallow Water equations with Coriolis force (1) but also a geostrophic equilibrium $g\nabla h + \omega \boldsymbol{u}^{\perp} = 0$. The proposed scheme (12) exactly preserves this initial condition by construction.
Figures 4a and 4b tend to confirm this property. Due to the wall-type boundary condition the solely entropic scheme (7) shows some oscillations on the wall for both unknowns but is accurate far from the boundaries. Finally, the HLLC scheme does not preserve the initial condition and converges to the lake-at-rest state.
In Figure 3 the fully discrete energy is not damaged by our schemes, unlike the HLLC scheme.

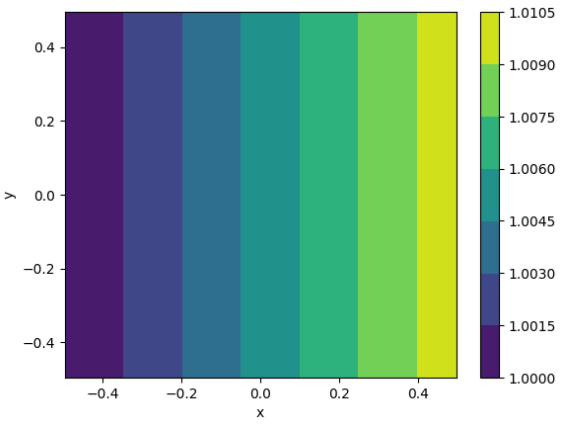

Figure 2: Initial water depth for the 1D equilibrium test case.

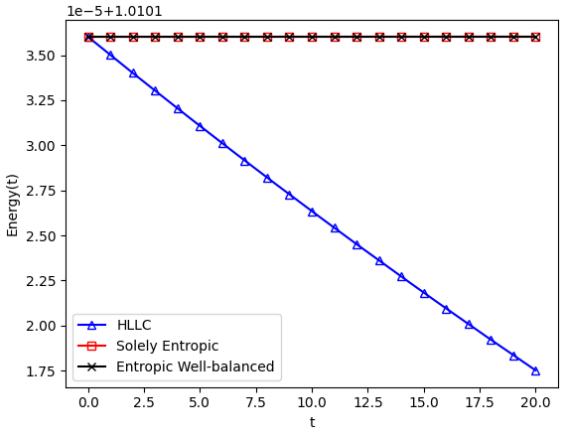

Figure 3: Energy of the system in function of time for the 1D equilibrium test case.

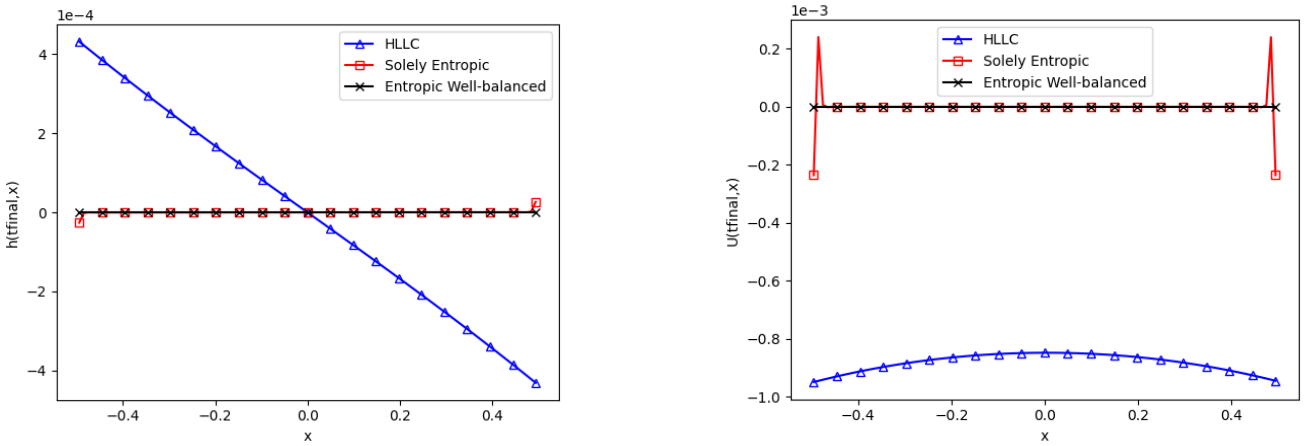

(a) Difference on Water depth

(b) Difference on Velocity u_y

Figure 4: Cross-section at $y = 0$ and $t = 20s$: deviation to the initial state for the 1D equilibrium test case.

5.2 Stationary vortex

We consider the test case introduced in [3] and defined by:

$$h(r) = \begin{cases} 1 + \dfrac{5\omega\epsilon}{2g} r^2, & \text{if } r \leq 0.2, \\ 1 + \dfrac{\omega\epsilon}{10g} - \dfrac{\omega\epsilon}{g}(0.3 - 2r + 2.5r^2) + \dfrac{\epsilon^2}{g}(3.5 - 20r + 12.5r^2 + 4\ln(5r)), & \text{if } 0.2 < r \leq 0.4, \\ 1 + \dfrac{\omega\epsilon}{5g} + \dfrac{\epsilon^2}{g}(4\ln(2) - 2.5), & \text{if } r > 0.4, \end{cases} \tag{24}$$

and

$$\boldsymbol{u}(r,\theta) = \begin{cases} -5\epsilon\ r\ {}^t(\sin(\theta), \cos(\theta)), & \text{if } r \leq 0.2, \\ -(2 - 5r)\epsilon\ {}^t(\sin(\theta), \cos(\theta)), & \text{if } 0.2 < r \leq 0.4, \\ 0, & \text{if } r > 0.4; \end{cases} \tag{25}$$

where r and θ are the polar coordinates in a domain with periodic boundary conditions. This initial condition can be seen on Figure 5. This is a stationary solution of the nonlinear Shallow Water equations with Coriolis force (1). Parameter ϵ is a measure of the nonlinearity: hence, we aim at assessing the scheme when ϵ goes to 0 as it becomes closer to the geostrophic equilibrium. Indeed, the definition of the water depth contains a second term that is related to the nonlinear advection in the equations. Then the smaller ϵ, the smaller the nonlinear term compared to the linear term.

We first take $\epsilon = 0.01$ and a final time of 200 s. For this test case, the solely entropic and entropic well-balanced schemes lead to similar results. We thus choose to showcase only one scheme on the 2D graphs, the entropic well-balanced one.

We can notice that the schemes we proposed exhibit better results than HLLC for the structure (Figures 6 and 7) and for the order of magnitude (Figure 8). Figure 9 shows that all schemes are energy-decreasing as expected.

Finally, let us make ϵ evolve and propose an indicator of the preservation of the stationary vortex

$$\frac{|\min(h_{final}) - \min(h_{init})|}{\max(h_{init}) - \min(h_{init})},$$

which tracks the lowest point of the vortex.

On Figure 10, for any value of ϵ, the HLLC scheme has the same behaviour since the scheme tries to reach the closest equilibrium in its kernel, namely the lake at rest. Meanwhile, our schemes capture the stationary vortex in a more efficient way as ϵ goes to 0 since the vortex becomes a quasi-equilibrium for the scheme.

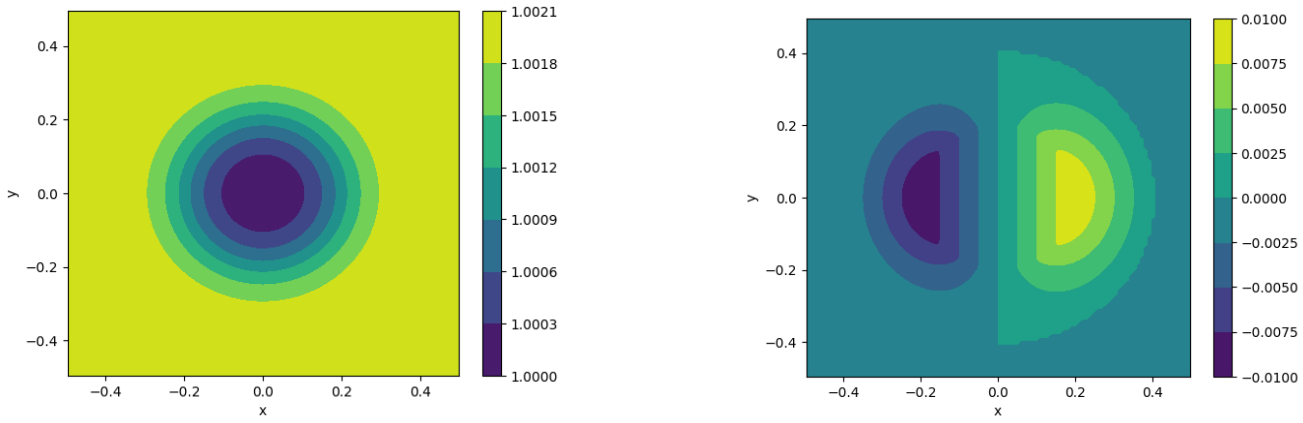

(a) Water depth

(b) Velocity v

Figure 5: Initial state of the stationary vortex for the stationary vortex test case.

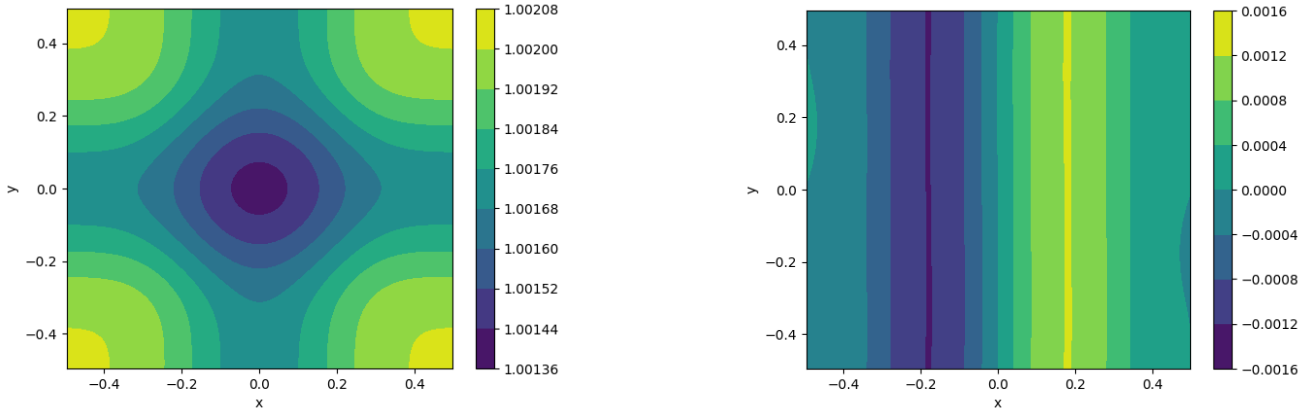

(a) Water depth

(b) Velocity u_y

Figure 6: HLLC solution at $t = 200s$ for the stationary vortex test case.

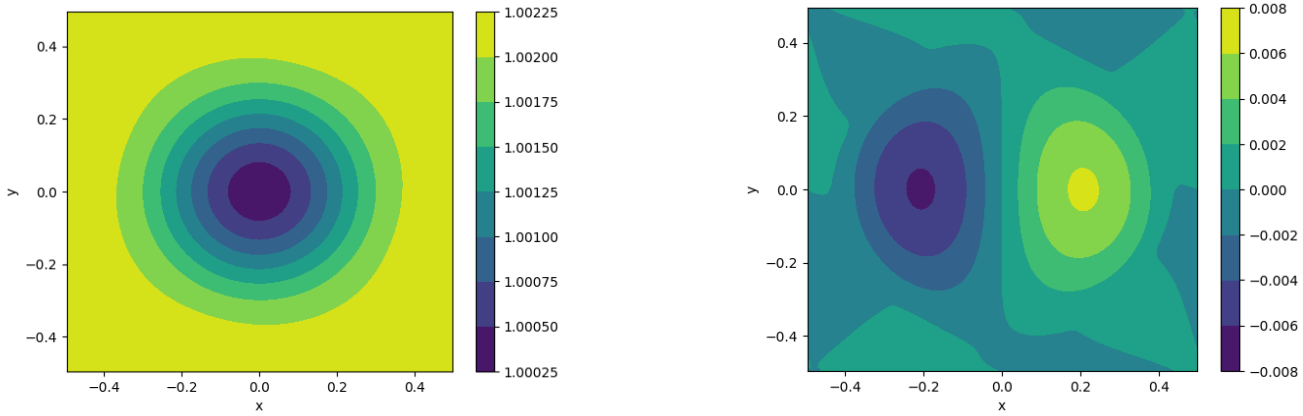

(a) Water depth

(b) Velocity u_y

Figure 7: Entropic well-balanced solution at $t = 200s$ for the stationary vortex test case.

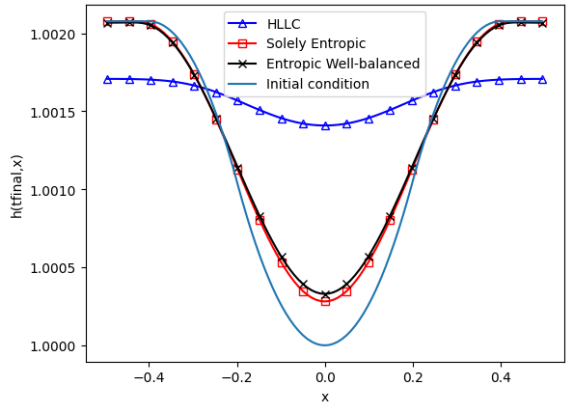

(a) Water depth

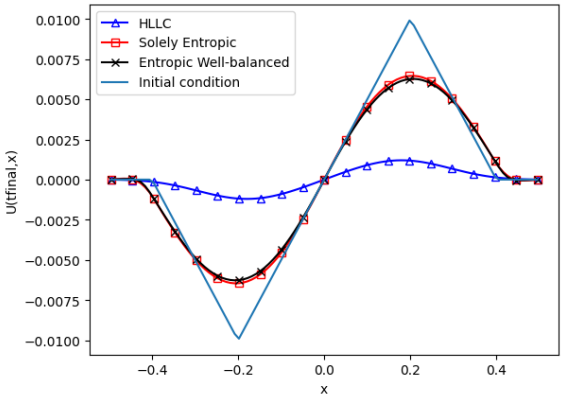

(b) Velocity u_y

Figure 8: Cross sections $y = 0$ of solutions at $t = 200s$ for the stationary vortex test case.

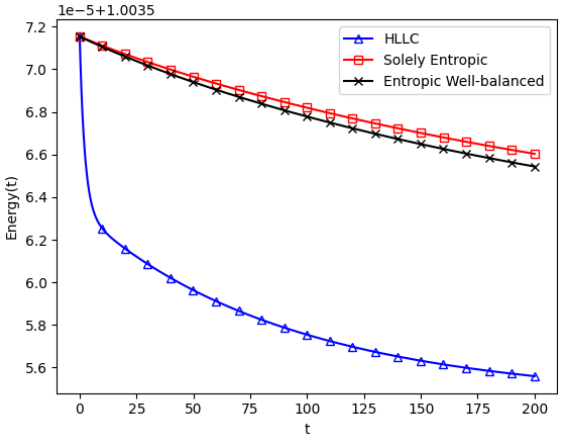

Figure 9: Energy of the system in function of time for $\epsilon = 0.01$ for the stationary vortex test case.

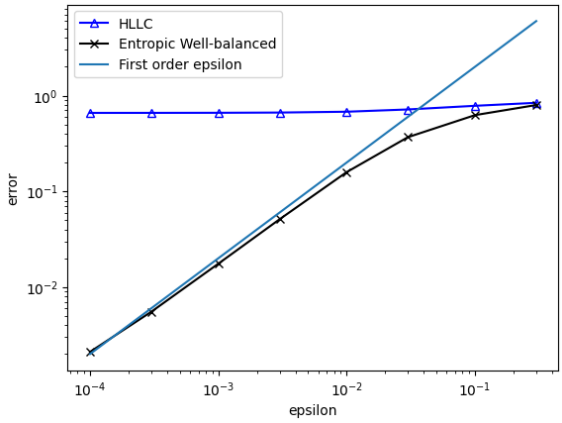

Figure 10: Relative error of water depth to initial state at $t = 200s$ for the different ϵ for the stationary vortex test case.

5.3 Translated vortex

This test case is a kind of mix of the two previous phenomena as we consider a translated vortex but based on a linear vortex. More precisely, the initial condition is defined by:

- the sum of (23) and (24) for h without considering ϵ^2 terms
- the sum of (23) and (25) for $\boldsymbol{u}$.

This initial condition (see Figure 11) is a geostrophic equilibrium and thus a stationary solution of the linear Shallow Water equations with Coriolis source term. The smaller ϵ, the closer the solution of the nonlinear problem to this stationary state. Here we set $\epsilon = 0.01$.
As for the 1D equilibrium test case, we enforce wall-type boundary condition for $x = -0.5$ and $x = 0.5$, and periodic boundary condition for $y = -0.5$ and $y = 0.5$. The slope of the free surface is ϵ, where ϵ is involved in the initial condition.
After 20 seconds, we observe on Figures 12 and 14 that the HLLC-scheme fails to preserve the structure of the initial state: the vortex is flattening out and the slope is decreasing.
On Figures 13 and 14, we see that the schemes we proposed capture the correct structure and the amplitude of the vortex.
On Figure 15, we note that the energy is also what one could expect from this superposition of solution: it is almost constant for the presented schemes, while it drops for the HLLC one.

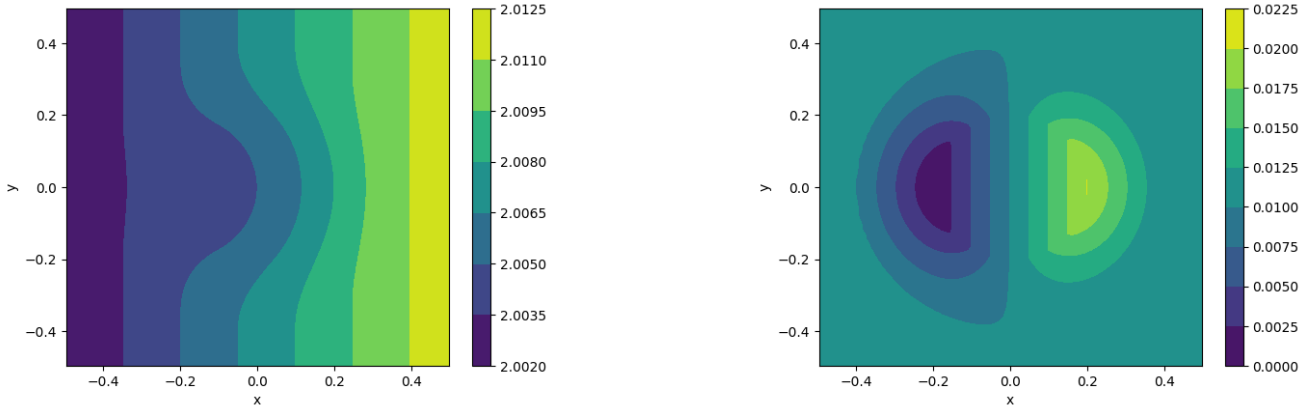

(a) Water depth

(b) Velocity u_y

Figure 11: Initial state of the translated vortex for the translated vortex test case.

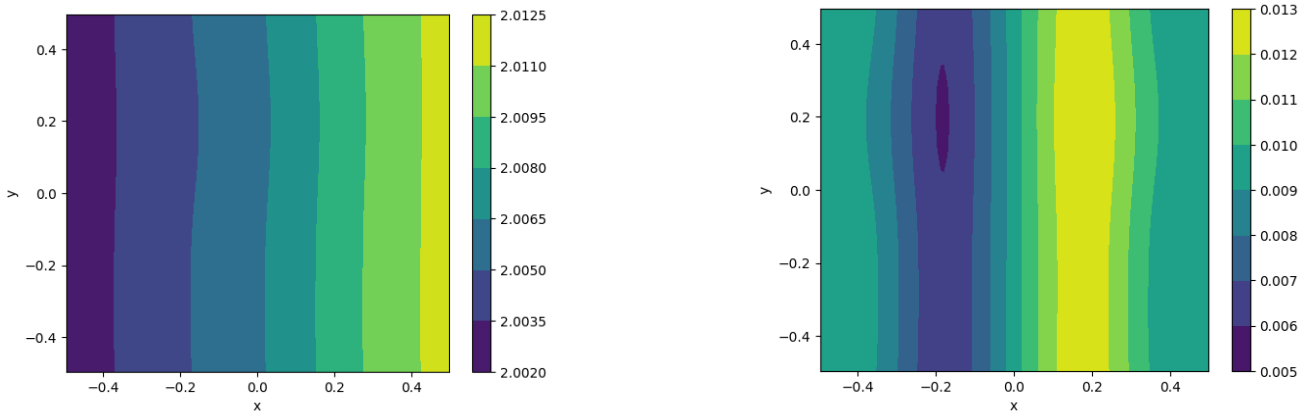

(a) Water depth

(b) Velocity u_y

Figure 12: HLLC solution at $t = 20s$ for the translated vortex test case.

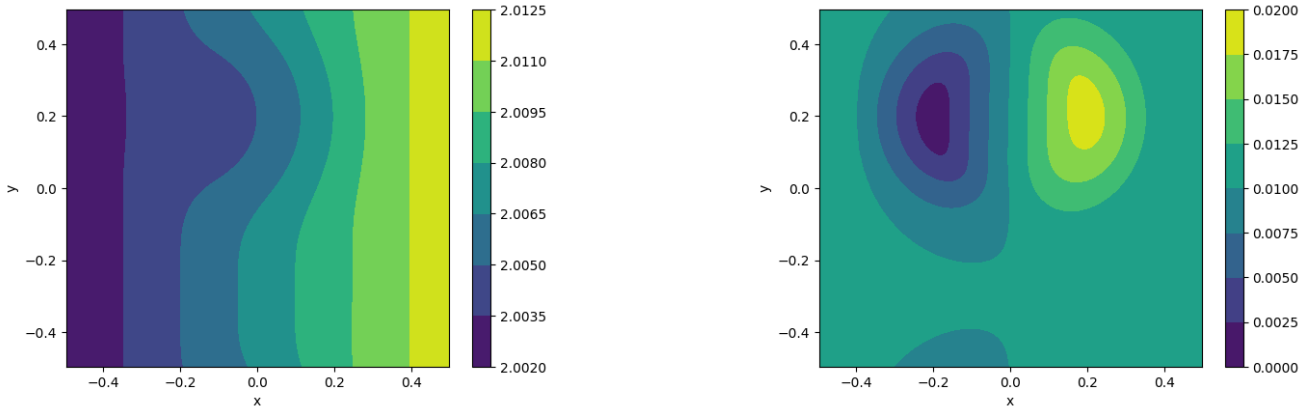

(a) Water depth

(b) Velocity v

Figure 13: Entropic Well-balanced solution at $t = 20s$ for the translated vortex test case.

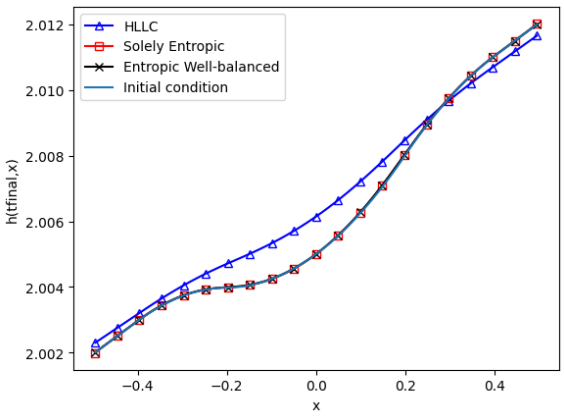

(a) Cross section $y = 0$ for initial condition and cross section $y = 0.2$ for numerical solutions

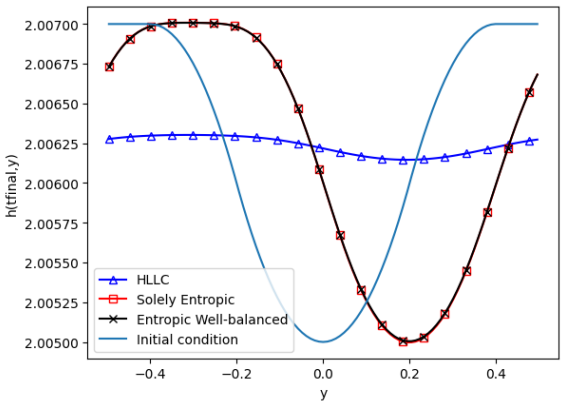

(b) Cross section $x = 0$

Figure 14: Water depth at $t = 20s$ for the translated vortex test case.

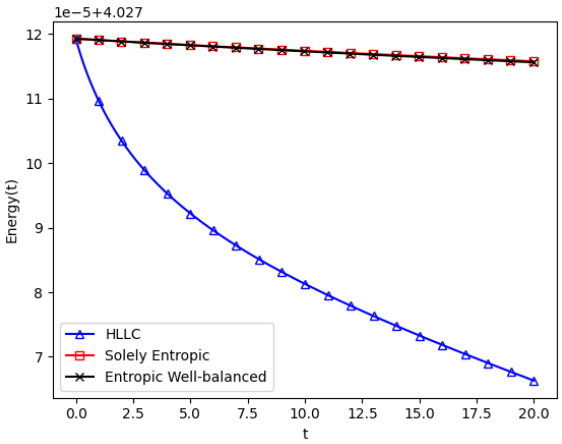

Figure 15: Energy of the system in function of time for the different schemes for the translated vortex test case.

5.4 Circular dam break

We consider a circular dam break on a rotating domain. At $t = 0$, the initial solution is given by

$$h(r) = \begin{cases} 2, & \text{if } r \leq 1, \\ 1, & \text{if } r > 1, \end{cases}, \qquad \boldsymbol{u}(r) = 0$$

This initial condition is very far from a geostrophic equilibrium. We consider Neumann boundary conditions. We expect some waves to be generated but to leave the domain until a geostrophic equilibrium remains. In this specific test case, the numerical diffusion coefficients are set to $\gamma = \nu = 0.25$.
On Figure 16, we compare the water height computed by the new scheme with 101 cells in each direction and by a classic HLLC scheme with 101, 401, 801 and 1601 cells at different times, from $1s$ to $100s$. We observe two types of behaviours: for short times, the decisive factor upon accuracy is the mesh size; for long times, the structure of the scheme becomes prominent. Indeed, Figure 16a shows that both schemes with the same resolution (101 cells) are overlapping. On Figure 16c, the former behaviour only applies to the leaving waves while on the centre of the domain, the geostrophic equilibrium appears which yields better results for our scheme. 1601 cells are required for the HLLC scheme to improve our results for longer times (see Figure 16f and Figures 17).

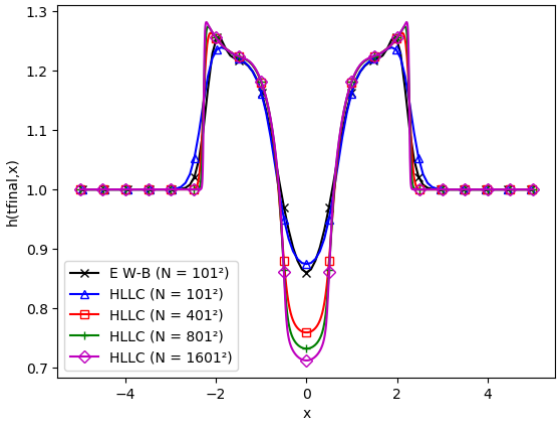

(a) $t = 1s$

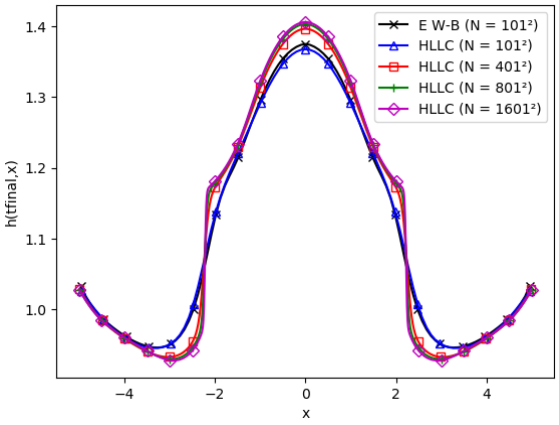

(b) $t = 4s$

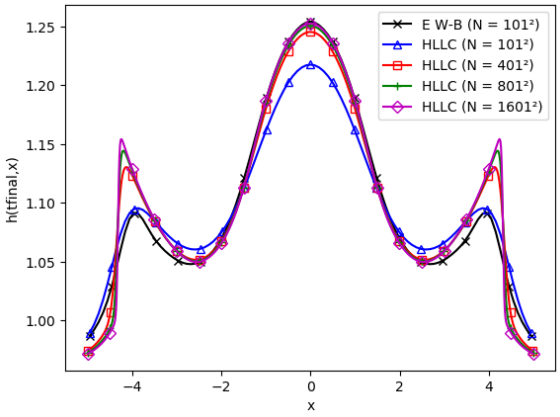

(c) $t = 6s$

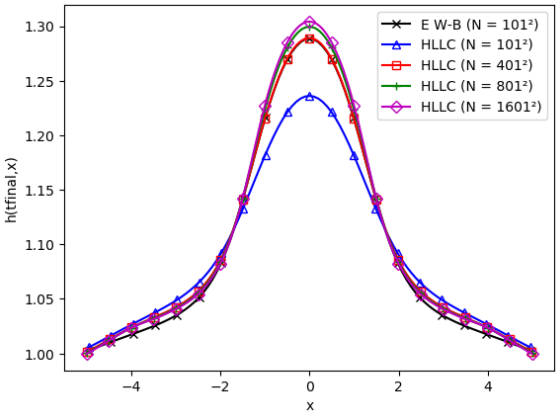

(d) $t = 10s$

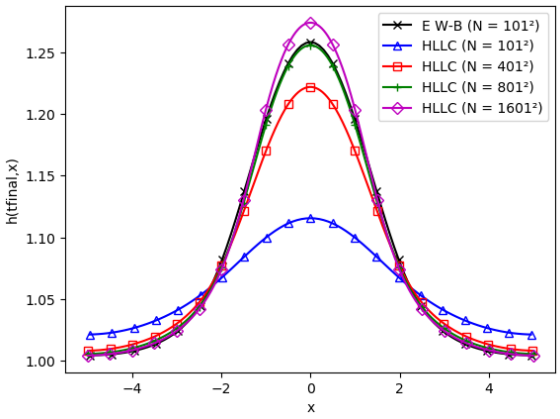

(e) $t = 40s$

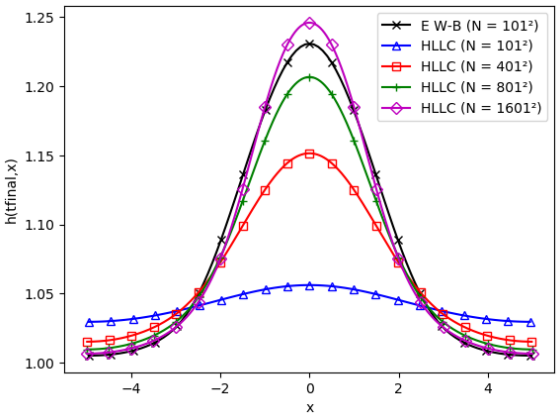

(f) $t = 100s$

Figure 16: Cross section in $y = 0$ of simulation results for the different schemes at different times for the circular dam break test case.

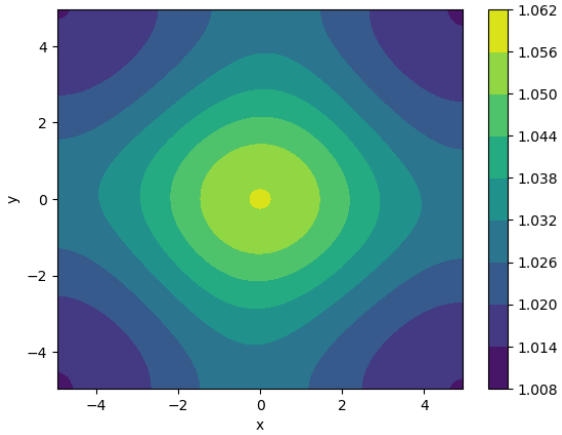

(a) HLLC scheme with 101 cells: water height

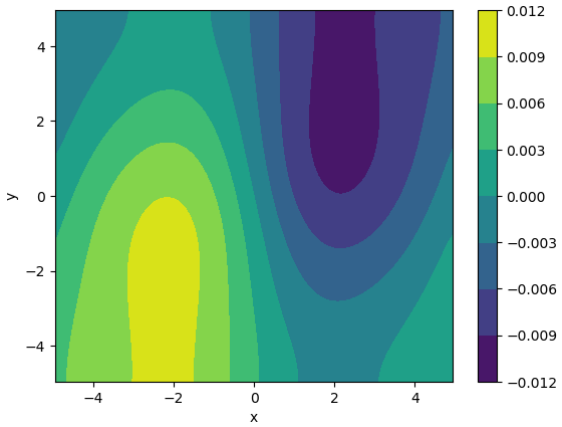

(b) HLLC scheme with 101 cells: u_y-velocity

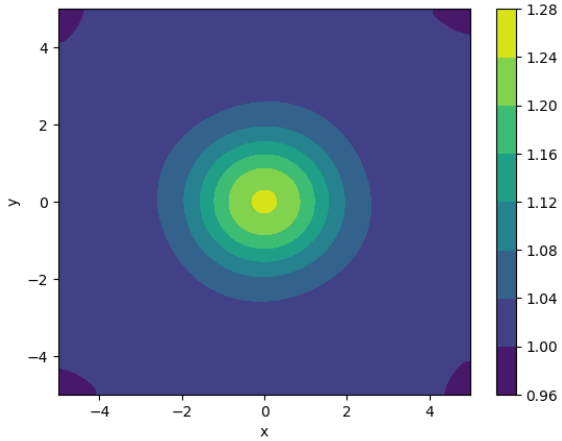

(c) HLLC scheme with 1601 cells: water height

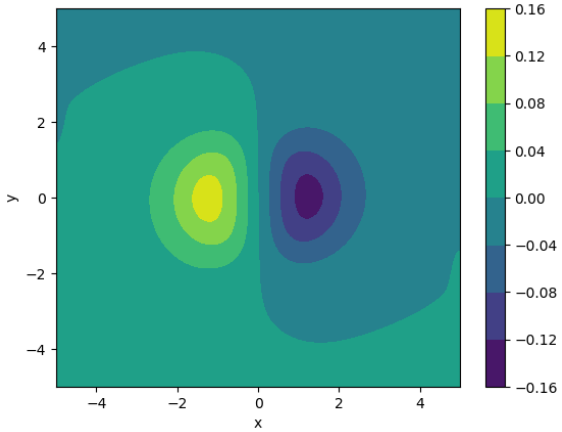

(d) HLLC scheme with 1601 cells: u_y-velocity

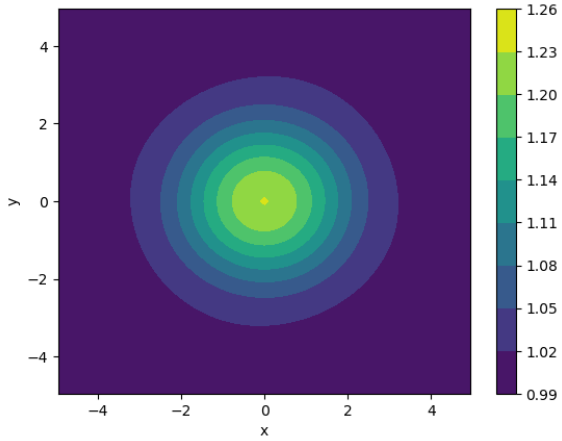

(e) Entropic Well-balanced scheme with 101 cells: water height

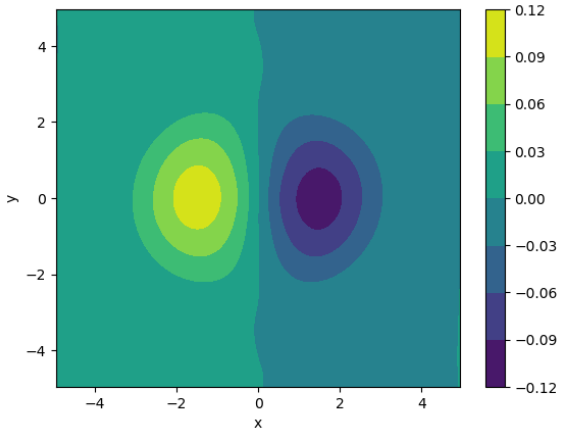

(f) Entropic Well-balanced scheme with 101 cells: u_y-velocity

Figure 17: Comparisons of u_y-velocity and water height at $t = 100s$ for the circular dam break test case.

6 Conclusion

In this work we derived a 9-point conservative colocated finite-volume scheme which is well-balanced and satisfies a semi-discrete entropy inequality for the shallow water equations with Coriolis force.
To design this scheme and obtain such properties, we kept the idea from [7] that the diffusion term in the mass flux is proportional to the geostrophic equilibrium on the edges. Observing that this equilibrium on edges induces an equilibrium at vertices (geostrophic equilibrium and vanishing divergence), we use duality relations to derive all remaining operators so that the energy estimate is satisfied and the scheme is well-balanced. Based on this first result, a conservative formulation was obtained.
Future works will be dedicated to the study of the fully discrete energy of the scheme and to the extension of this strategy to triangular meshes. The study of the dispersion relations of the presented scheme should also be investigated, see [25].

References

[1] E. Audusse, H. Do Minh, P. Omnes, and Y. Penel. Analysis of modified Godunov type schemes for the two-dimensional linear wave equation with Coriolis source term on cartesian meshes. *Journal of Computational Physics*, 373:91–129, 2018.

[2] E. Audusse, V. Dubos, A. Duran, N. Gaveau, Y. Nasseri, and Y. Penel. Numerical approximation of the shallow water equations with Coriolis source term. *ESAIM: Proceedings and Surveys*, 70:31–44, June 2021.

[3] E. Audusse, R. Klein, and A. Owinoh. Conservative discretization of Coriolis force in a finite volume framework. *Journal of Computational Physics*, 228(8):2934–2950, 2009.

[4] A. Bermudez and M. Vazquez-Cendon. Upwind methods for hyperbolic conservation laws with source terms. *Computers and Fluids*, 23(8):1049–1071, 1994.

[5] C. Berthon, M. M'Baye, M. H. Le, and D. Seck. A well-defined moving steady states capturing Godunov-type scheme for Shallow-water model. *International Journal on Finite Volumes*, 15, 2020.

[6] F. Bouchut. *Nonlinear stability of finite volume methods for hyperbolic conservation laws, and well-balanced schemes for sources*, volume 2/2004. Birkhäuser Basel, 2004.

[7] F. Bouchut, J. Le Sommer, and V. Zeitlin. Frontal geostrophic adjustment and nonlinear wave phenomena in one-dimensional rotating shallow water. Part 2. High-resolution numerical simulations. *Journal of Fluid Mechanics*, 514:35–63, 2004.

[8] M. Castro, J. Antonio López, and C. Pares. Finite volume simulation of the geostrophic adjustment in a rotating shallow-water system. *SIAM Journal on Scientific Computing*, 31:444–477, 01 2008.

[9] A. Chertock, M. Dudzinski, A. Kurganov, and M. Lukácová-Medvidóvá. Well-balanced schemes for the shallow water equations with Coriolis forces. *Numerische Mathematik*, 138:939–973, 2018.

[10] F. Couderc, A. Duran, and J.-P. Vila. An explicit asymptotic preserving low Froude scheme for the multilayer shallow water model with density stratification. *Journal of Computational Physics*, 343:235–270, 2017.

[11] J. R. Edwards. Reflections on the early development of the "AUSM family" of Riemann solvers. *Shock Waves*, 29(5):601–609, 2019.

[12] R. Eymard, T. Gallouët, and R. Herbin. *Finite Volume Methods*, volume 7 of *Handbook of Numerical Analysis*. Elsevier, 2000.

[13] L. Gosse. *Computing qualitatively correct approximations of balance laws*, volume 2. Springer, 2013.

[14] J. Greenberg and A. LeRoux. A well-balanced scheme for the numerical processing of source terms in hyperbolic equations. *SIAM Journal on Numerical Analysis*, 33(1):1–16, 1996.

[15] S. Jin. Efficient asymptotic-preserving (AP) schemes for some multiscale kinetic equations. *SIAM Journal on Scientific Computing*, 21(2):441–454, 1999.

[16] R. J. LeVeque. *Finite volume methods for hyperbolic problems*. Cambridge Texts in Applied Mathematics. Cambridge University Press, Cambridge, 2002.

[17] M.-S. Liou. A Sequel to AUSM: AUSM+. *Journal of Computational Physics*, 129(2):364–382, 1996.

[18] M.-S. Liou and C. J. Steffen. A new flux splitting scheme. *Journal of Computational Physics*, 107(1):23–39, 1993.

[19] X. Liu, A. Chertock, and A. Kurganov. An asymptotic preserving scheme for the two-dimensional shallow water equations with Coriolis forces. *Journal of Computational Physics*, 391:259–279, 2019.

[20] J. Maddison, D. Marshall, C. Pain, and M. Piggott. Accurate representation of geostrophic and hydrostatic balance in unstructured mesh finite element ocean modelling. *Ocean Modelling*, 39(3–4):248–261, 2011.

[21] M. Parisot and J.-P. Vila. Centered-potential regularization for the advection upstream splitting method. *SIAM Journal on Numerical Analysis*, 54(5):3083–3104, 2015.

[22] T. Ringler, J. Thuburn, J. Klemp, and W. Skamarock. A unified approach to energy conservation and potential vorticity dynamics for arbitrarily-structured C-grids. *Journal of Computational Physics*, 229(9):3065–3090, 2010.

[23] J. Thuburn, T. Ringler, W. Skamarock, and J. Klemp. Numerical representation of geostrophic modes on arbitrarily structured C-grids. *Journal of Computational Physics*, 228(22):8321–8335, 2009.

[24] E. F. Toro. *Riemann Solvers and Numerical Methods for Fluid Dynamics*. Springer, 2009.

[25] R. A. Walters, E. Hanert, J. Pietrzak, and D. Le Roux. Comparison of unstructured, staggered grid methods for the shallow water equations. *Ocean Modelling*, 28(1):106–117, 2009. The Sixth International Workshop on Unstructured Mesh Numerical Modelling of Coastal, Shelf and Ocean Flows.

[26] R. A. Walters, E. M. Lane, and E. Hanert. Useful time-stepping methods for the Coriolis term in a shallow water model. *Ocean Modelling*, 28(1):66–74, 2009. The Sixth International Workshop on Unstructured Mesh Numerical Modelling of Coastal, Shelf and Ocean Flows.

[27] H. Zakerzadeh. The RS-IMEX scheme for the rotating shallow water equations with the Coriolis force. In C. Cances and P. Omnes, editors, *Finite Volumes for Complex Applications VIII - Methods and Theoretical Aspects*, pages 199–207. Springer, 2017.

[28] V. Zeitlin. *Geophysical fluid dynamics: understanding (almost) everything with rotating shallow water models*. Oxford University Press, 2018.